Supplementary Information

Polynary Energy Harvesting and Multi-Parameter Sensing in the Heatwave Environment of Industrial Factory Buildings by the Integrated Triboelectric-Thermoelectric Hybrid Generator

Lin Fang[a], Chen Chen[a], Haonan Zhang[a], Xinbo Tu[a], Zixun Wang[a], Wen He[a], Shengnan Shen[b], Mingzai Wu[a], Peihong Wang[a, *], Li Zheng[c, *], Zhong Lin Wang[d, e, f *]

[a] School of Materials Science and Engineering, Energy Materials and Devices Key Lab of Anhui Province for Photoelectric Conversion, Anhui University, Hefei, Anhui 230601, China

[b] Hubei Key Laboratory of Electric Manufacturing and Packaging Integration (Wuhan University), Wuhan University, Wuhan, Hubei 430072, China

[c] College of Mathematics and Physics, Shanghai Key Laboratory of Materials Protection and Advanced Materials in Electric Power, Shanghai University of Electric Power, Shanghai 200090, China

[d] Beijing Institute of Nanoenergy and Nanosystems, Chinese Academy of Sciences, Beijing 101400, China

[e] School of Materials Science and Engineering Georgia Institute of Technology Atlanta, GA 30332, USA

[f] Yonsei Frontier Lab, Yonsei University, Seoul 03722, Republic of Korea

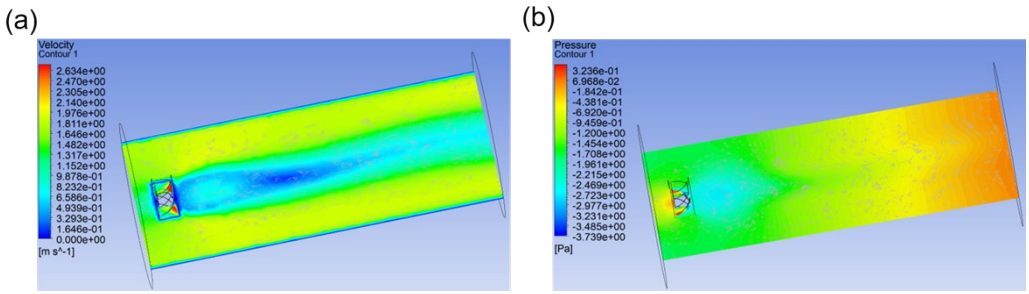

Figure S1. The velocity (a) and pressure (b) contours simulation under wind-blown of 5 m/s by ANAYS.

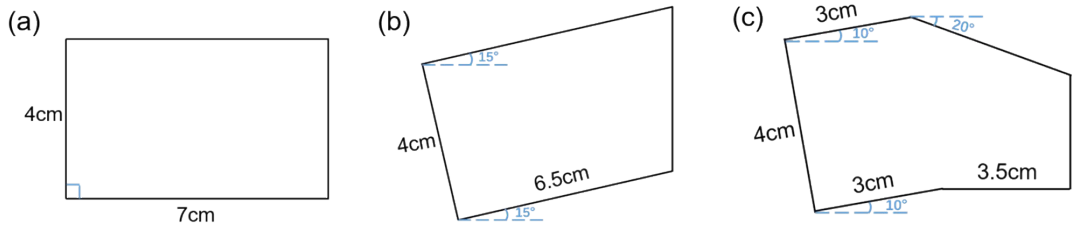

Figure S2. The schematic and actual dimension parameters of three different polymer film. (a) Rectangle shape (R-shape); (b) Trapezoid-shape (T-shape); (c) Designed-shape (D-shape).

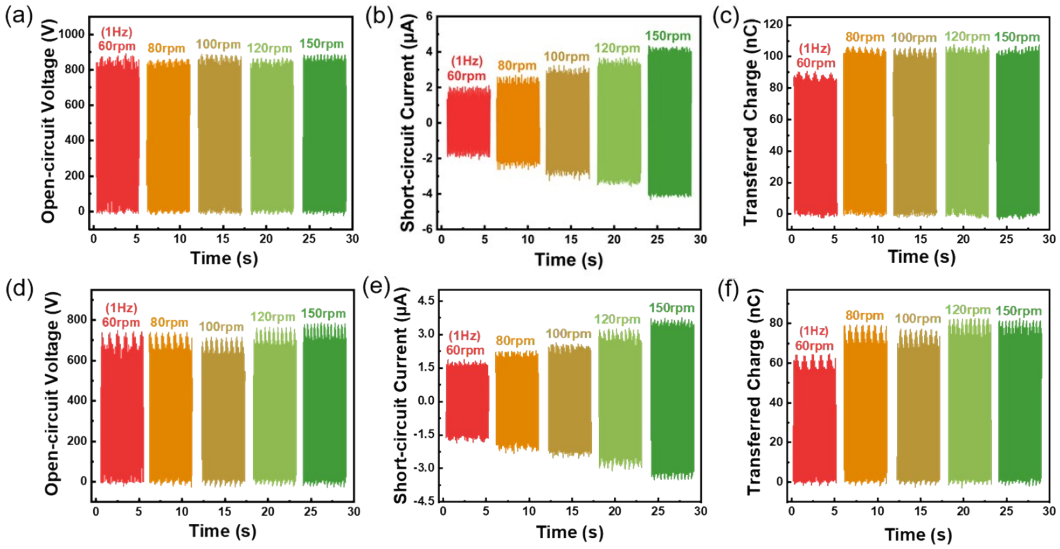

Figure S3. The basic output performance of FR-TENG based on T-shape (a~c) and R-shape (d~f) FEP film.

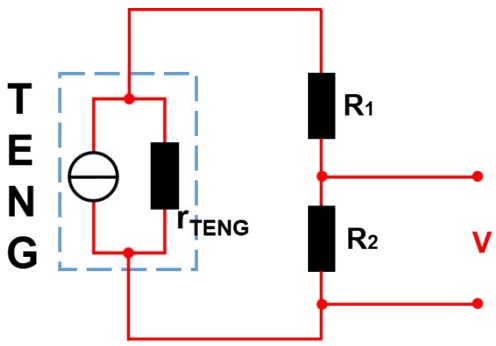

Figure S4. The voltage division circuit for open-circuit voltage V_{OC} measurement of FR-TENG.

Note S1: When the open-circuit voltage value of TENG exceeds 200 V, it is difficult to directly measure with 6514. Under this scenario, in order to protect the equipment and get a more reliable output, we can take advantage of a voltage division circuit to measure the open-circuit voltage of TENG by the idea of dividing the voltage through series resistance. It can be seen from **Figure S4** above that the open-circuit voltage of FR-TENG can be referred without considering the heat loss, and the detailed parameters and expressions are as follows:

$$R_1 \gg R_2 \gg r_{TENG} \tag{1}$$

$$R_{1=}10\ \mathrm{G\Omega} \tag{2}$$

$$R_{2=}1\ \mathrm{G\Omega} \tag{3}$$

$$V_{OC} = \frac{V}{R_2} \times (R_1 + R_2) = 11V \tag{4}$$

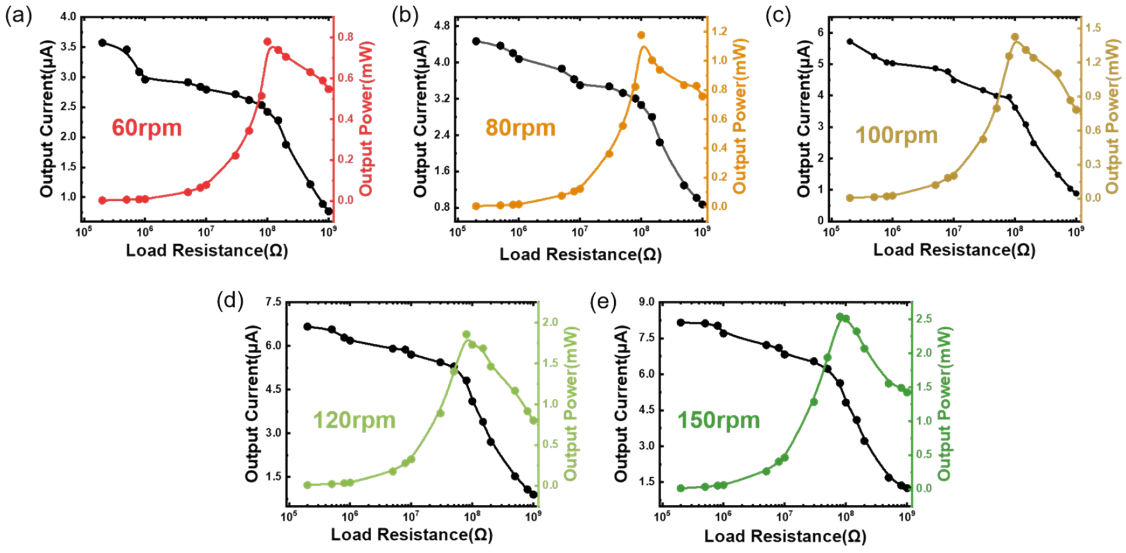

Figure S5. The peak output power of FR-TENG under different rotation speeds.

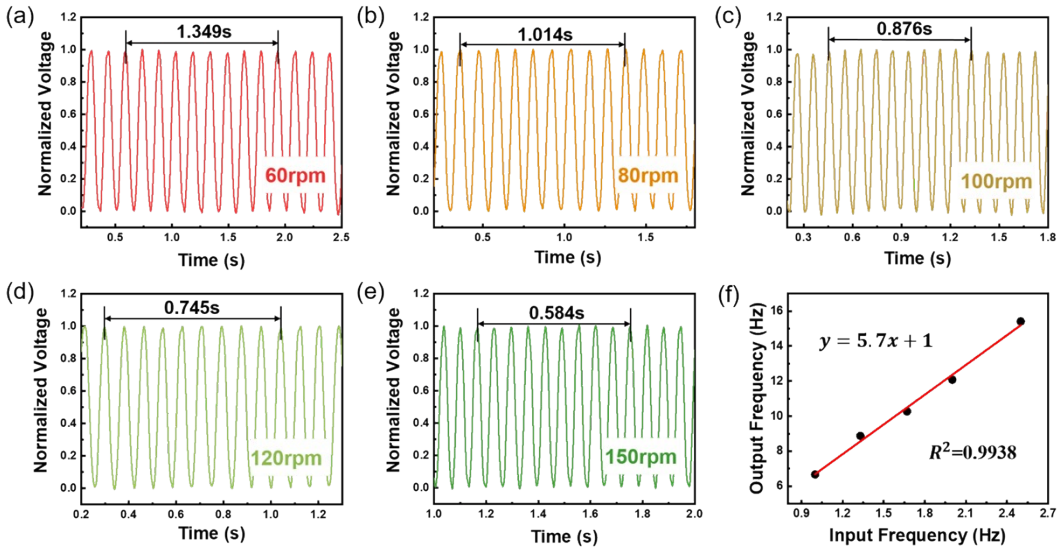

Figure S6. The output frequency calculation of FR-TENG under different rotation speeds (a~e). (f) The linear relationship between input and output frequency of FR-TENG.

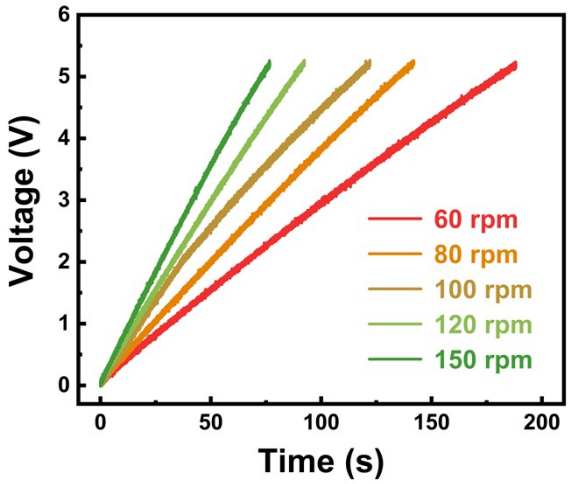

Figure S7. Charging a 47 μF capacitor by FR-TENG through a rectifier under different rotation speeds.

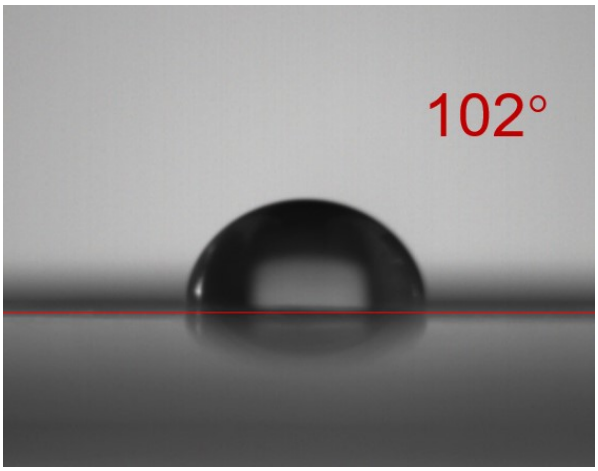

Figure S8. The water contact angle photo of hydrophobic FEP film (thickness of 100 μm).

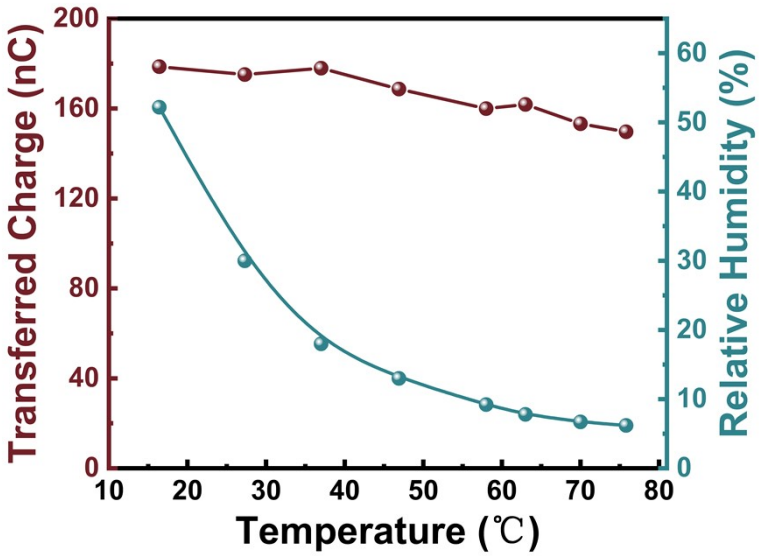

Figure S9. The transferred charge output of FR-TENG under different environmental temperatures.

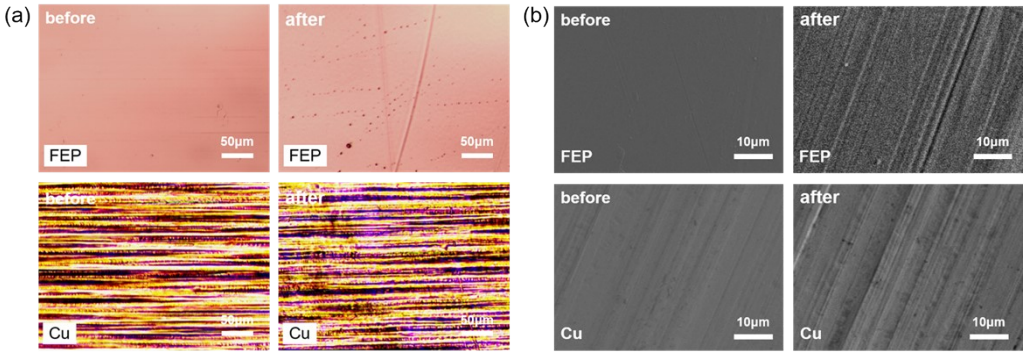

Figure S10. The metallographic microscope images (a) and SEM images (b) of Cu and FEP before and after rubbing.

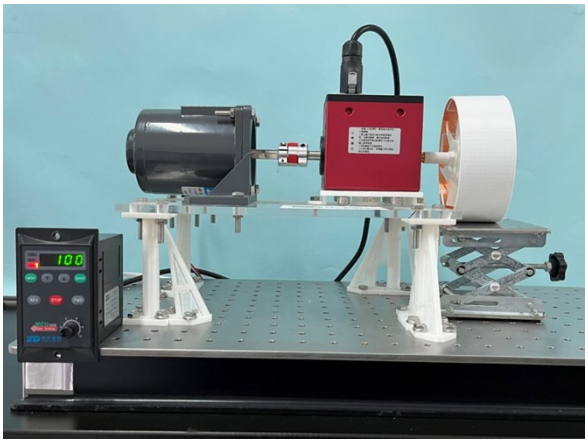

Figure S11. The test platform for torque measurement.

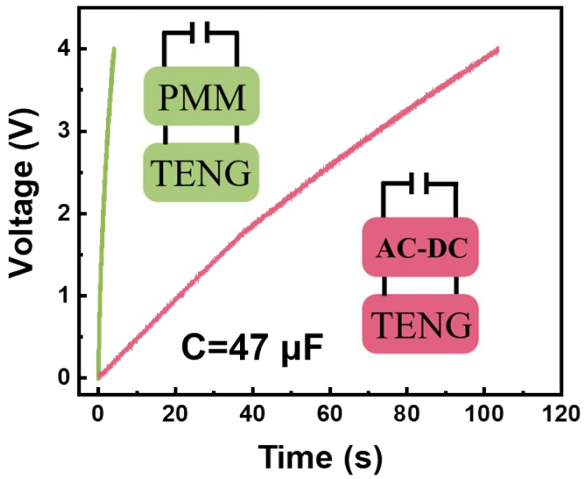

Figure S12. The charging capacity comparison of FR-TENG between through PMM and AD-DC rectifier under 100 rpm rotation speed.

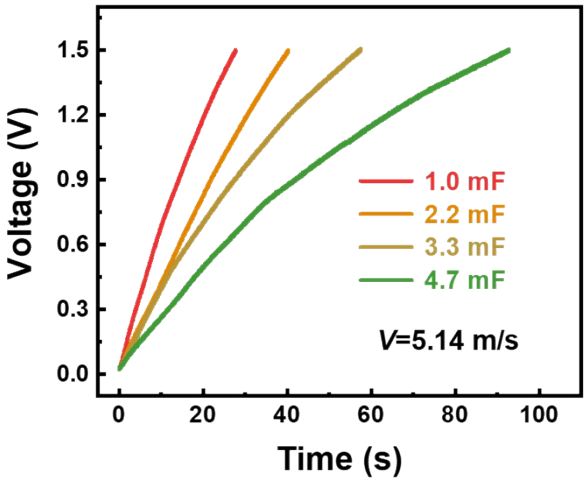

Figure S13. Charging different capacitors by FR-TENG through PMM under 5.14 m/s wind speed.

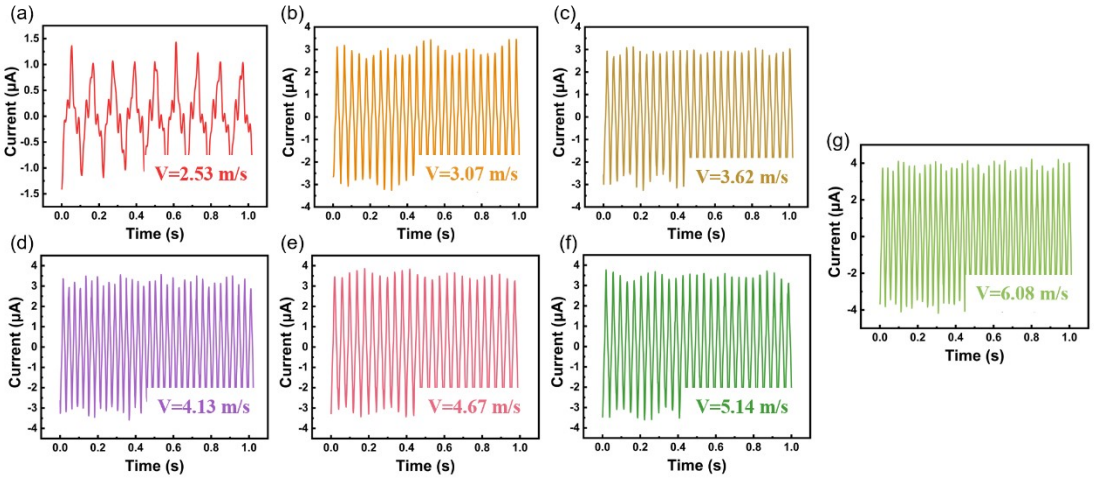

Figure S14. The load current output of FR-TENG connected with matched resistance under different wind speeds.

Note S2: The detailed calculation process is as follows:

$$\eta = \frac{P_{TENG}}{P_{wind}} \tag{5}$$

in which,

$$P_{wind} = \frac{1}{2} S \rho V^3 \tag{6}$$

$$P_{TENG} = \frac{\int_0^T i^2(t) R dt}{T} \tag{7}$$

$$\text{T=1 s} \tag{8}$$

where S is the effective cross-sectional area blown by the wind, which is calculated as 0.0177 m^2 for the FR-TENG.

In the most literature involving the calculation of TENG energy conversion efficiency, the integration duration T is not clearly stated. In theory, it can be the duration of a single output signal or multiple output cycles. However, in the actual calculation process, the selection of integration duration will affect the calculation results of energy conversion efficiency. This is because the output of TENG in the working process is not absolutely stable, but there will be relative fluctuation as shown in Figure S14. Here, we choose the time of ~1 s as the integration duration containing multiple output signals, which can improve the accuracy of the calculation results to a certain extent.

For ease of calculation, we assume the wind blows vertically through FR-TENG from

the horizontal plane. ρ is the density of air, which is 1.2928 kg/m^3 in the standard condition, here it is approximately estimated as 1.2 kg/m^3 in view of temperature and other ambient factors. V is the wind speed. P_{TENG} represents average power of FR-TENG.

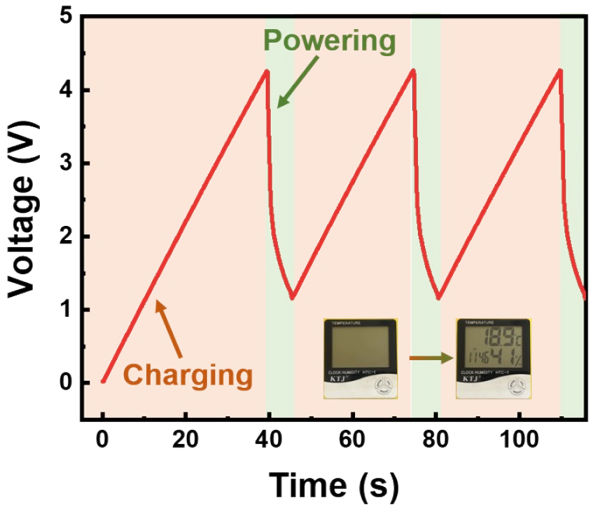

Figure S15. Driving a hygrothermograph intermittently through AC-DC rectifier under 120 rpm rotation speed.

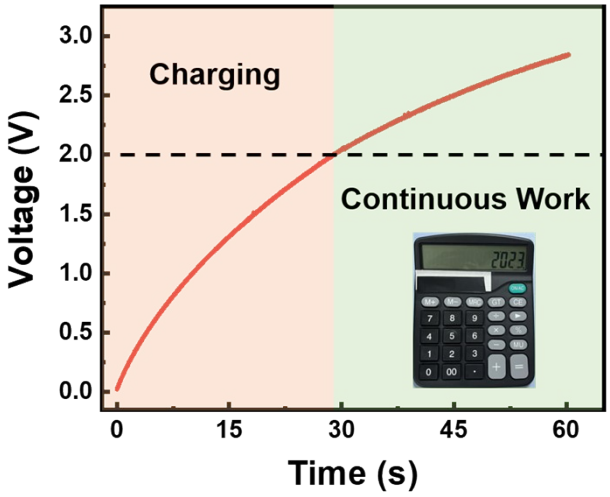

Figure S16. Powering an electronic calculator continuously through PMM under 150 rpm rotation speed.

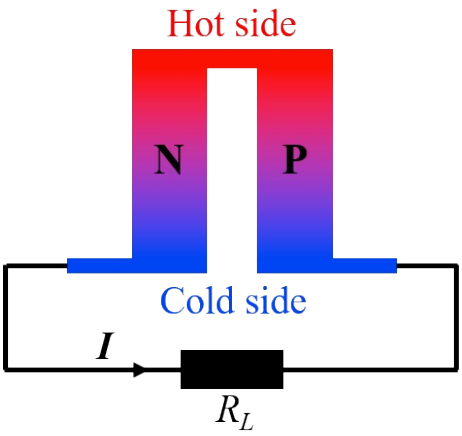

Figure S17. The electricity generation principle of ThEG under temperature difference.

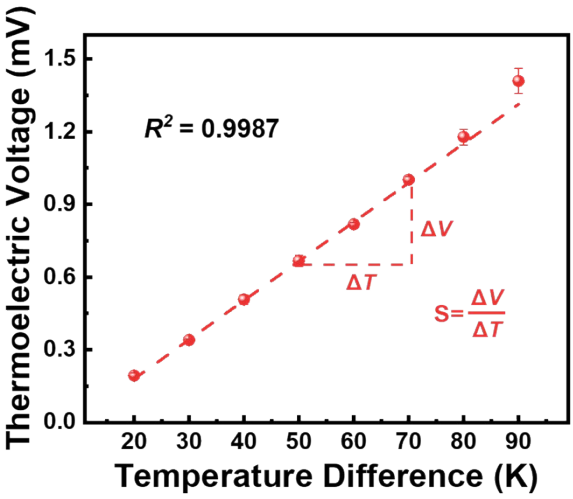

Figure S18. The Seebeck coefficient of constantan ($Cu_{55}Ni_{45}$).

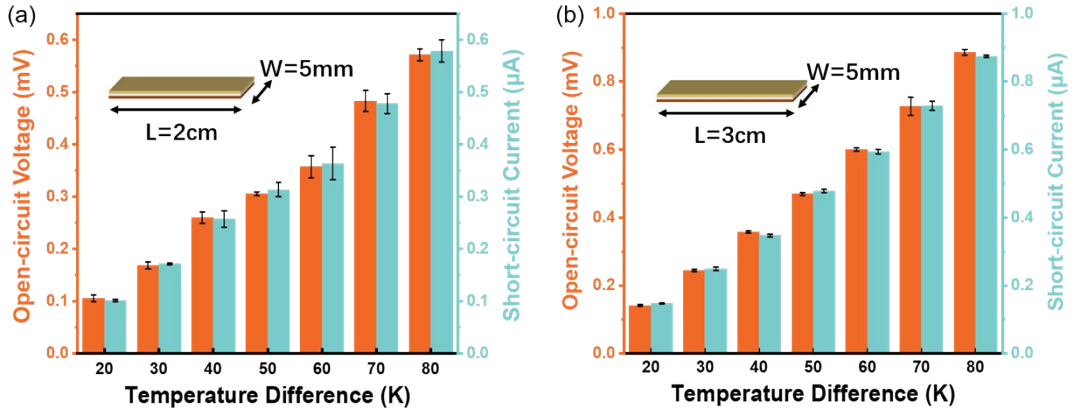

Figure S19. The output performance of iThEG with different lengths of (a) 2 cm and (b) 3 cm (The width of iThEG is kept as 5 mm).

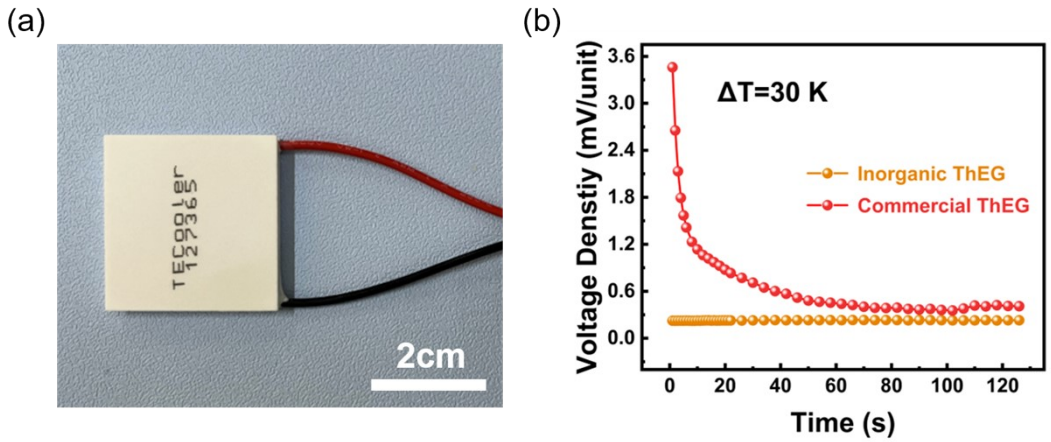

Figure S20. (a) The photo of commercial ThEG module (TEG-127365), (b) The voltage density comparison between commercial ThEG and inorganic ThEG under temperature difference of 30 K.

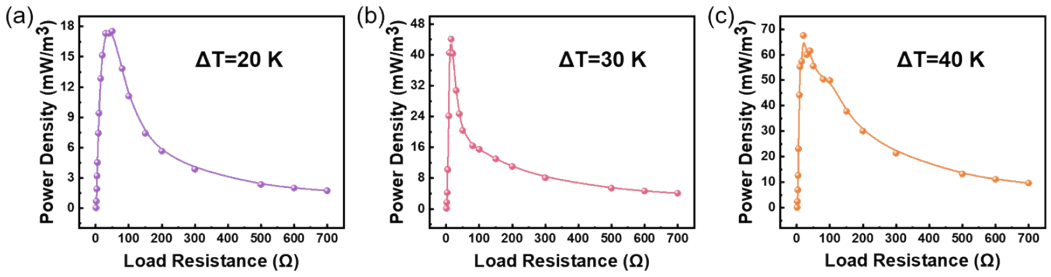

Figure S21. The output power density of iThEG under different temperature differences.

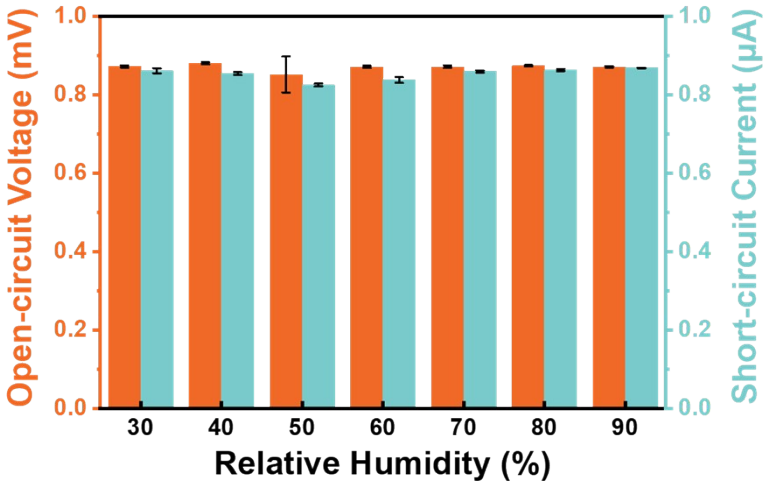

Figure S22. The output stability of iThEG under different relative humidity conditions.

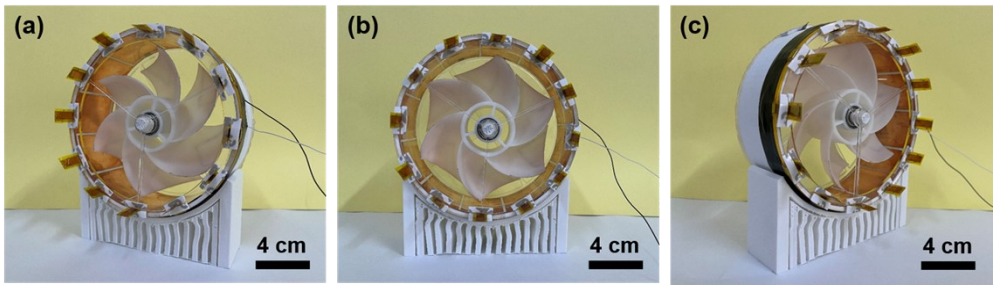

Figure S23. The digital photos of the hybrid generator from different angles.

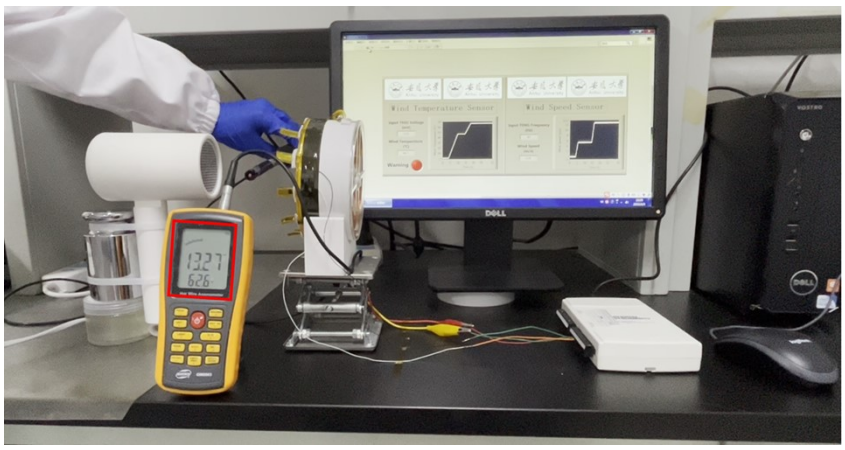

Figure S24. The hot-wind sensing information detected by commercial anemometer.

Table S1. Comparison between hybrid generators integrating TENG and ThEG

	Name	Output performance	Work condition	Device size	Auxiliary facility
Ref. [1]	AR-TENG	499.3 mW	f=10 Hz	d=30 cm	Al alloy heat sink; epoxy resin adhesive; polyurethane (PUR)
	ThEG	31.9 mW	ΔT=22 K	32(units)×40×40 mm	
Ref. [2]	TENG	238.9 mW	f=16.67 Hz	d=14.5 cm	heat transfer plate
	ThEG	14.5 mW	ΔT=7 K	8(units)×40×40×4 mm	
Ref. [3]	r-TENG	0.47 mW/cm^2	f=8.33 Hz	d=8 cm	
	TMENG	16.59 mW	V=500 rpm	16 cm^2	
Ref. [4]	CS-TENG	69.32 mW/m^2	f=1 Hz; F=10 N	16 cm^2	
	ThEG	1.967 mW	ΔT=15 K	TEC1-12706	
Ref. [5]	TENG	4.55 mW/m^2	f=1.79 Hz	45×45 mm	Phase change material (PCM)
	ThEG	10.43 mW/m^2	ΔT=2.5 K	161 Bi_2Te_3 units	
Ref. [6]	TENG	24.34 mW/m^2	f=30 Hz	38×38 mm	PU
	ThEG	110 μW	ΔT=10 K	72 Bi_2Te_3 units	
Ref. [7]	TENG	61.6 W/m^3	V=10.2 m/s		heat sink
	ThEG	147.6 W/m^3	ΔT=40 K		
Ref. [8]	TENG	0.79 mW	V=12 m/s		heat sink; micro heat pipe array
	ThEG	0.39 W	V=16 m/s		
Ref. [9]	O-TENG	U_{OC}~5.85 V I_{SC}~0.35 μA	f=1 Hz; a=30°	20×70 mm	
	MTEG	U_{OC}~1.821 V I_{SC}~7.382 mA	V=6 m/s; T_h=30 °C		
Ref. [10]	Disk-TENG	204.4 μW	f=14.1 Hz	d=38 mm	
	ThEG	136 μW	ΔT=50 K	72 Bi_2Te_3 units	
This work	FR-TENG	352.6 mW/m^2	f=2.5 Hz	d=130 mm	
	iThEG	0.7 W/ m^3	ΔT=70 K	(30×5×0.1 mm)/unit	

Note:

f: working frequency;

ΔT: temperature difference between hot side and cold side of the ThEG device;

V: rotation speed (rpm) or fluid (wind/water) speed (m/s);

F: pressure exerted on the TENG device;

a: swing amplitude;

T_h: temperature of the hot side of ThEG device;

d: diameter of the circular device.

	Name	Input Energy/Power	Output Energy/Power	Integration Duration (T)	Efficiency (η)
Ref.[11]	SS-TENG	$E_{in} = mg(h_1 - h_2)$	$E_{out} = \int I(t)^2 R dt$	One external trigger (~60 s)	$\eta_{max} = 28.2\%$
Ref.[12]	ES-TENG	$E_{in} = mg\Delta h$	$E_{out} = \int I(t)^2 R dt$	One external trigger (~65 s)	$\eta_{max} = 29.7\%$
Ref.[13]	Cylindrical-TENG	$E_{in} = 2mgh_0$	$E_{out} = \int_0^T I_t^2 R dt$	One external trigger (~80 s)	$\eta = 5.7\%$
Ref.[14]	DEL-WD-TENG	$E_{in} = \int_0^t \frac{A \cdot N}{k} dt$	$E_{out} = \int_0^t I^2 R dt$		$\eta = 10.3\%$
Ref.[15]	D-TENG	$P_{wind} = \frac{1}{2} S\rho V^3$	$P_{output} = \frac{\int_0^T i^2 R dt}{T}$		$\eta_{max} = 67\%$
This Work	FR-TENG	$P_{wind} = \frac{1}{2} S\rho V^3$	$P_{output} = \frac{\int_0^T i^2 R dt}{T}$	~1 s	$\eta_{max} = 37.2\%$

Table S2: The energy conversion efficiency calculation of different TENG devices

Note:
m: mass of the swing component;
g: gravitational acceleration;
h_1, h_2: heights between the center of gravity and the cylinder shell bottom;
Δh: height difference between the center of gravity at the highest and final states;
h_o: distance between the rotor barycenter and the bearing center;
A: torque generated by rotational friction;
N: rotational speed;
K: a constant with a value of 9549;
S: effective cross-sectional area blown by the wind;
ρ: density of air;
V: wind speed.

References

[1] O. Yang, C. Zhang, B. Zhang, L. He, W. Yuan, Y. Liu, X. Li, L. Zhou, Z. Zhao, J. Wang, Z. L. Wang, *Energy Tech* **2022**, *10*, 2101102.

[2] X. Wang, Z. L. Wang, Y. Yang, *Nano Energy* **2016**, *26*, 164.

[3] Y. Wu, S. Kuang, H. Li, H. Wang, R. Yang, Y. Zhai, G. Zhu, Z. L. Wang, *Adv. Mater. Technol.* **2018**, *3*, 1800166.

[4] I. Kim, J. Yun, S. Jo, Y. Kim, H. Roh, D. Kim, *Intl J of Energy Research* **2022**, *46*, 1444.

[5] M.-K. Kim, M.-S. Kim, S.-E. Jo, Y.-J. Kim, *Smart Mater. Struct.* **2016**, *25*, 125007.

[6] S. Jo, I. Kim, J. Byun, N. Jayababu, D. Kim, *Adv. Mater. Technol.* **2021**, *6*, 2000752.

[7] M. Ma, Z. Zhang, Q. Liao, G. Zhang, F. Gao, X. Zhao, Q. Zhang, X. Xun, Z. Zhang, Y. Zhang, *Nano Energy* **2017**, *39*, 524.

[8] C. Liu, C. Zhao, J. Liu, J. Wang, Y. Wang, Y. Fan, K. Zhao, B. Shan, Z. Qu, K. Ma, M. Xu, X. Pan, *International Journal of Green Energy* **2021**, *18*, 1302.

[9] C. Liu, G. Qu, B. Shan, R. Aranda, N. Chen, H. Li, Z. Zhou, T. Yu, C. Wang, J. Mi, M. Xu, *Materials Today Sustainability* **2023**, *21*, 100301.

[10] D. Lee, I. Kim, D. Kim, *Nano Energy* **2021**, *82*, 105696.

[11] T. Jiang, H. Pang, J. An, P. Lu, Y. Feng, X. Liang, W. Zhong, Z. L. Wang, *Advanced Energy Materials* **2020**, *10*, 2000064.

[12] Z. Lin, B. Zhang, Y. Xie, Z. Wu, J. Yang, Z. L. Wang, *Adv Funct Materials* **2021**, *31*, 2105237.

[13] Y. Feng, T. Jiang, X. Liang, J. An, Z. L. Wang, *Applied Physics Reviews* **2020**, *7*, 021401.

[14] D. Fang, G. Gu, W. Zhang, G. Gu, C. Wang, B. Zhang, G. Cheng, Z. Du, *Nanoenergy Advances* **2023**, *3*, 236.

[15] S. Yong, J. Wang, L. Yang, H. Wang, H. Luo, R. Liao, Z. L. Wang, *Advanced Energy Materials* **2021**, *11*, 2101194.